MANSOURA JOURNAL OF CHEMISTRY
Official Journal of Faculty of Science, Mansoura University, Egypt
E-mail: scimag@mans.edu.eg ISSN: 2974-4938

Unveiling the Potential of Hydrazonoyl Cyanide Dyes for High-Efficiency Dye-Sensitized Solar Cells: A Computational Odyssey

Amal R. Mostafa, Safa A. Badawy, Ehab Abdel-Latif*, Ahmed Fekri, Ahmed A. Fadda, Mohamed R. Elmorsy, Soha M. Abdelmageed

Chemistry Department, Faculty of Science, Mansoura University, 35516 Mansoura, Egypt

** Emal: ehabattia00@gmx.net, Tel:+201002529365*

Received: 22/4/2024
Accepted: 30/4/2024

Abstract: Dye-sensitized solar cells (DSSCs) are a promising renewable energy technology, and the development of high-performance sensitizer dyes is key to improving their power conversion efficiency. This work utilized synthesis and theoretical studies to investigate ten new hydrazonoyl cyanide-based organic dyes (**AML-1-4**) as photosensitizers for DSSC applications. The effects of systematic variations in the donor, π-spacer, and acceptor/anchoring units on optical, electronic, and photovoltaic properties were analyzed. The absorption spectra, frontier molecular orbital distributions, intramolecular charge transfer characteristics, light-harvesting efficiency (LHE), injection driving force (ΔG_{inject}), dye regeneration (ΔG_{reg}), recombination driving force (ΔG_{rec}), and open-circuit voltage (V_{OC}) were calculated. Among the proposed dyes, **AML-4**, which contains a carbazole as a strong donor and a chlorohydrazonoyl cyanide acceptor, demonstrated the most red-shifted absorption, narrowest bandgap (1.90 eV), superior electron delocalization, most favorable alignment of frontier orbital energies for efficient electron transfer processes, and greater G_{Inject} and G_{Reg} values compared to the other sensitizers. Comprehensive simulations provide an in-depth understanding of structure-function relationships to advance molecular engineering strategies for developing optimal hydrazonoyl cyanide-based organic photosensitizers. This study lays the theoretical foundation for the experimental realization of high-performance dyes tailored through judicious structural modifications.

keywords: Acetohydrazonoyl cyanide organic dyes; sensitizers; DSSCs; DFT

1.Introduction

Dye-sensitized solar cells (DSSCs) have gained significant attention as promising alternatives to conventional silicon-based solar cells because of their potential for low-cost fabrication and high efficiency under a wide range of lighting conditions. These solar cells operate based on the principle of light absorption by a sensitizer dye, which generates excited electrons that are subsequently injected into the semiconductor material to produce electricity. The concept of dye-sensitized solar cells was first proposed by O'Regan and Grätzel in the early 1990s and inspired by natural photosynthesis processes in plants. Since then, extensive research has been dedicated to the development of efficient and stable DSSCs [1-3]. Briefly, DSSC devices consist of four main partitions: the photoanode (FTO-coated glass), sensitizer layer (consisting of organic or inorganic dye molecules), and an electrolyte system [4]. The key component of DSSCs is the sensitizer dye, which plays a crucial role in the light absorption and electron injection processes. Various sensitizer dyes have been explored, including organic dyes, metal complexes, and semiconductor quantum dots [5]. Computational modeling serves as a powerful tool for understanding the working principles of complex solar cells and rationally guiding their optimized design prior to experimental trial-and-error [6]. Theoretical simulations based on quantum chemical methods, such as density functional theory (DFT), can provide atomistic insights into solar

cell operational mechanisms under illumination [7]. Molecular engineering of light-absorbing materials and interfaces is enabled by evaluating the impact of strategic structural modifications on photoconversion efficiency parameters [8]. It elucidates the relationships between material compositions, interface energetics, and device architectures on photovoltaic performance indicators, such as short-circuit current, open-circuit voltage, fill factor, and efficiency [9]. Therefore, computational efforts strongly complement and guide the targeted experimental realization of solar cells with enhanced efficiency. Overall, theoretical photophysics simulations significantly advance the rational design and fundamental understanding of solar cell materials and devices to achieve cost-effective and scalable solar energy harvesting [10]. Carbazole (Cz) and its counterpart are highly regarded as powerful electron donors in DSSCs. This is mainly due to the presence of the aliphatic groups attached to carbazole group, which helps to reduce aggregation on semiconductor surfaces such as TiO_2. Carbazole-based dyes are known to exhibit impressive efficiencies mainly due to their exceptional electron-donating capabilities and the endless opportunities for enhancing a wide range of properties [11]. Acetohydrazonoyl cyanide (also known as AcHC) has been studied and used in various applications including dye-sensitized solar cells (DSSCs). DSSCs are a type of solar cell that utilize a dye molecule to absorb light and convert it into electricity. AcHC can be used as a sensitizer in DSSCs owing to its ability to absorb light in the visible region of the electromagnetic spectrum. As a sensitizer, it can transfer absorbed energy to the underlying semiconductor material, which initiates the electron transfer process and generates an electric current [12-14]. This study focuses on the synthesis and rational molecular engineering of new acetohydrazonoyl cyanide-based organic dyes, termed **AML-1-4**, as photosensitizers for DSSCs. The specific design and performance of DSSCs can vary depending on various factors such as the choice of sensitizer, electrolyte composition, and cell configuration. AcHC has been investigated as a potential sensitizer owing to its favorable optical and electronic properties such as a high molar absorption coefficient and suitable energy levels for electron injection. In this study, we systematically investigated the effects of incorporating a strong donor segment (ethylcarbazole), π-spacer, and acceptors (acetohydrazonoyl cyanide derivatives) on the optical, electrochemical, and photovoltaic characteristics of **AML-1-4** dyes. (DFT) calculations provide insights into the correlation between molecular structure and efficiency. The absorption spectra, frontier molecular orbital energies, electron density distributions, and intramolecular charge transfer properties were analyzed. Photovoltaic parameters including light-harvesting efficiency, driving forces for injection and dye regeneration, charge recombination losses, and open-circuit voltage were estimated. Comprehensive theoretical modeling sheds light on the structure-function relationships to explain and predict the photoconversion efficiencies of the sensitizer series. This work demonstrates that molecular engineering through judicious functionalization of donors, spacers, and acceptors is a viable strategy for developing highly efficient organic dyes for dye-sensitized solar cells.

2. Results and Discussion

Synthesis and Characterization. The starting material (**1**) was synthesized successfully with a favorable yield, following the procedure outlined in a previously published research article **[15] (Scheme 1)**. The methylene group in the synthesized cyanoacetamide derivative **1** exhibited reactivity in electrophilic coupling reactions with aryl diazonium chlorides **(2a-d) [16]**. Specifically, it was coupled with different diazotized anilines, including aniline, 4-toluidine, 4-anisidine, and 4-chlorobenzaldehyde, in pyridine in a temperature range of 0-5ºC. This led to the formation of the corresponding hydrazone derivatives **AML-1-4 (Scheme 1**). The chemical structures of **AML-1-4** were validated and confirmed using elemental and spectroscopic analyses. The IR spectrum of **AML-1** showed an characterization absorption bands at 3386, 2215 and 1674 cm^{-1}, corresponding to the following groups (NH), (CN), in addition to a peak for the carbonyl groups (C=O). The ^1H NMR spectrum showed

the aromatic protons were exhibited as triplet, doublet of doublet and doublet signals at δ 7.11- 8.40 ppm. In case of, ^{1}H NMR spectrum of **AML-2** showed a singlet signal at δ 2.29 ppm related to the methyl group (CH_3), and the characterized two amino groups (-NH) showed a singlet signal at 9.99 and 11.81 cm^{-1}. Furthermore, **AML-2** mass analysis revealed a molecular ion peak at m/z 395 (32.81%), which corresponded to the molecular formula of $C_{24}H_{21}N_5O$. In the context of C^{13} analysis, **AML-2** manifested approximately 24 discernible signals. The methyl moiety was clearly identified by a chemical shift recorded at 20.49 ppm, while the carbonyl functionality was resolved at 159.55 ppm. The ^{1}HNMR of **AML-3** revealed a singlet signal at δ 3.75 ppm related to the methoxy group (OCH_3), additionally two singlet signals at 9.95 and 11.82 ppm characteristic to the protons of NH groups. For C^{13}, **AML-3** exhibited about 24 signals, the characterized signal for methoxy group appeared 55.34 ppm at and for carbonyl group at 159.69 ppm. The mass analysis of **AML-3** revealed a molecular ion peak at m/z = 411, aligned with the molecular formula $C_{24}H_{21}N_5O_2$. The ^{1}H NMR spectrum of **AML-4** revealed the existence of 11 aromatic resonances, appearing as triplet, doublet, doublet of doublet, and multiplet peaks within the chemical shift range of 7.17-8.38 ppm. Additionally, the amino groups protons (–NH) were observed as two singlets, positioned at 10.09 and 11.92 ppm. During C^{13} analysis, **AML-4** displayed approximately 23 clear signals, suggesting its structural complexity. The carbonyl group stood out with a characteristic chemical shift of 159.22 ppm. Dye-sensitized solar cells (DSSCs) offer a promising and cost-effective solar cell technology. To enhance their performance, it is crucial to develop highly efficient organic sensitizer dyes. In this study, we focused on investigating a series of new carbazole dyes, namely **AML-1-4**, for their potential use in DSSCs. By employing spectroscopic and computational methods, we systematically analyzed the molecular structures, optical properties, and photovoltaic parameters of these dyes. Our findings revealed that modifying the donor, π-bridge, and acceptor components of the dyes had a significant impact on various key factors. These factors included light absorption, charge transfer, and electron injection capabilities. Through careful analysis and experimentation, we were able to understand how these modifications influenced the overall performance of the dyes in DSSCs.

Optical properties. **Figure 1** displays the absorption spectra of **AML-1-4** when exposed to the DMF solution. The corresponding values obtained from the experiment can be found in **Table 1.**

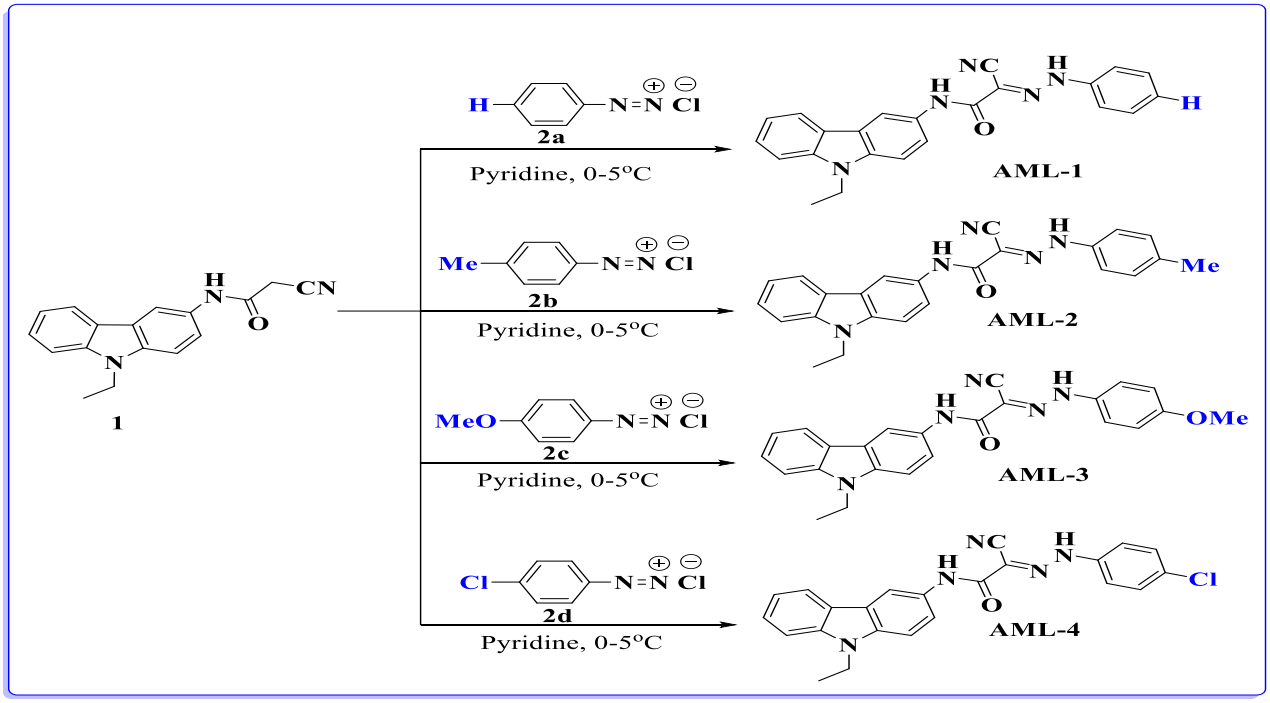

Scheme 1 synthesis of hydrazone derivatives **AML-1-4.**

Table 1. Optical parameters of sensitizers **AML-1-4.**

Sensitizer	λ_{max} (nm)	ε (10^4 $M^{-1}cm^{-1}$)	λ_{onset} (nm)	*$ExperimentalE_{0-0}$ (eV)
AML-1	**(293, 412)**	**(2.81, 4.14)**	**472**	**2.62**
AML-2	**(288, 467)**	**(3.04, 2.71)**	**550**	**2.25**
AML-3	**(281, 486)**	**(3.47, 2.90)**	**565**	**2.19**
AML-4	**(283, 537)**	**(2.99, 3.37)**	**650**	**1.90**

Fig.1 depicts the UV-vis absorption spectra of acetohydrazonoyl cyanide **AML-1-4,** while Table 1 provides a detailed summary of the results. The appearance of bands in the shorter-wavelength regions can be attributed to the π-π* electron transition of the chromophore. Furthermore, the absorption band observed between 410 and 550 nm indicates the occurrence of intramolecular charge transfer (ICT) from the donors to their associated acceptors [17]. The maximum absorption wavelengths (**λ_{max}**) were recorded for **AML-1-4** and furthermore, the energy gap (E_{0-0}) can be estimated from the onset of the lowest energy band in the UV–visible absorption spectrum [18], which decreases in the following order: **AML-4 (1.90 eV) < AML-3 (2.19 eV) < AML-2 (2.25 eV) < AML-1 (2.62 eV)**. The higher molar extinction coefficient for **AML-4 (**3.37×10^4 $M^{-1}.cm^{-1}$**)** compared with that for other sensitizers indicates a good ability for light harvesting. Sensitizer **AML-4**, bearing an ethyl carbazole moiety with 4-chlorohydrazonoyl cyanide as an acceptor and electron-withdrawing group, exhibited the largest red-shifted maximum absorption compared to the other sensitizers. This bathochromic shift is attributed to enhanced electron delocalization enabled by the π-conjugated framework and the presence of an electron-withdrawing group linker in the A-π structure [19]. Sensitizers **AML-2** and **AML-3** demonstrated a greater bathochromic shift relative to **AML-1.** This can be attributed to the presence of methoxy (-OCH_3) and methyl (-CH_3) groups on the aromatic ring of the sensitizers, which can cause a redshift in the absorption wavelength. This redshift occurs because of the electron-donating nature of the methoxy and methyl groups, which leads to an increase in electron density around the central chromophore. **AML-1** had the largest energy gap (2.62 eV), which can be attributed to the structure of the former dye, which has less conjugation owing to the absence of a substituent on the benzene ring. Acetohydrazonoyl cyanide **AML-1-4** sensitizers have smaller energy gaps, making them suitable candidates for DSSCs [20].

By modifying the acceptor groups, our novel carbazole dyes (**AML-1-4**) could harvest light significantly more efficiently. Consequently, dye-sensitized solar cells can deliver superior quality outcomes. Molecular engineering of the dye structure is crucial for optimizing light absorption, and the acceptor design is responsible for the significant light absorption of the sensitizers.

Theoretical calculations. To gain insights into the impact of the donor, π-spacer, and acceptor/anchoring groups on the geometry of carbazole sensitizers **AML-1-4**, computational investigations were conducted. The calculations were performed using Gaussian 09 software, employing the B3LYP/6-311g (d,p) basis set [21]. The optimized geometries of **AML-1-4** are visually represented in **Fig.2**, while Table 2 provides a comprehensive overview of the dihedral angles and bond lengths corresponding to each dye. The dyes exhibited a propeller-like arrangement of π-bridges, characterized by specific dihedral angles and bond lengths. These structural characteristics are crucial for facilitating an efficient charge transfer. By employing computational modeling, valuable insights into the relationship between structure and function can be obtained, aiding the future design of sensitizers based on acetohydrazonoyl cyanide [22].

For further insights, **Table 2** indicated the bond lengths of **AML-1** as **D1** (2.02 Å), **D2** (1.45 Å), **AML-2** as **D1** (1.76 Å), **D2** (2.43 Å), **AML-3** as **D1** (1.49 Å), **D2** (1.44 Å) and **AML-4** as **D1** (1.19 Å), **D2** (1.42 Å), respectively**.** It is obvious that the **AML-3-4** sensitizers are shorter and more stable than the other sensitizers [23]. The bond lengths (**D1 and D2**) for **AML-4** connected to the cholroacetohydrazonoyl cyanide varied widely, with a minimum bond length (**D1**) of 1.19 Å and a bond length (**D2**) of 1.42 Å. This result

shows that the presence of an auxiliary electron-withdrawing group leads to an increase in conjugation stability across the sensitizer. In the case of the chloroacetohydrazonoyl cyanide sensitizer **AML-1-4**, the dihedral angles (**D1**) among the donor and π-linker were exhibited as the following 154.34°, 156.87°, 177.90°, and -179.27°. These values indicate a nearly planar geometry for the sensitizer. The dihedral angle (**D2**) of these sensitizers between the donor and π-bridge were changed from 150.70 ° to 179.80°, leading to a planar structure between the π-spacers and the various acceptor groups [24]. Sensitizer **AML-4** had a coplanar arrangement between the donor/spacer and acceptor units. This planar conformation enabled extended electron delocalization over the entire dye framework. This increased conjugation allows for more efficient intramolecular charge transfer (ICT) and the lowest optical bandgap (Eg) among the dyes, making it promising for light harvesting in dye-sensitized solar cells [25].

The frontier molecular orbitals (FMO). To gain a deeper understanding and examine the electrical properties of the enhanced dyes, **Fig. 3** shows the frontier molecular orbital (FMO) energy level diagram for the four designed dyes, depicting their HOMO/LUMO levels relative to the TiO_2 CB edge and electrolyte redox potential [26].

Effective sensitizers require suitable HOMO/LUMO positions to facilitate electron injection from the dye into the TiO_2 CB after photoexcitation [27, 28]

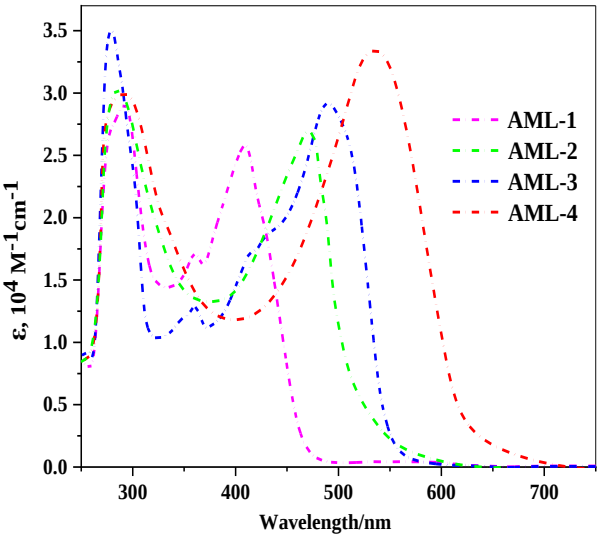

Fig.1. UV-Vis absorption spectra of carbazole sensitizers **AML-1-4.**

Table2: Dihedral angle and bond length results for carbazole sensitizers **AML-1-4.**

Sensitizers	Dihedral angle (°)		Bond length (Å)	
	D1	D2	D1	D2
AML-1	154.34	150.70	2.02	1.45
AML-2	156.87	175.56	1.76	2.43
AML-3	177.90	176.23	1.49	1.44
AML-4	-179.27	179.80	1.19	1.42

As depicted in **Table 3,** the HOMO levels of all the dyes under study (ranging from -6.27 to -5.49 eV) are below the redox potential of I^-/I_3^-, indicating that the oxidized sensitizer **AML-1-4** can be efficiently regenerated by the redox couple during the dye regeneration process [29]. Their LUMO energy levels (ranging from -3.57 to -3.67 eV) lie above the CB of TiO_2 which guarantees that the excited state electrons can be readily transferred during the charge injection process [30]. In the current investigation, the bandgap of the current architecture molecules **(AML-1-4)** was found to be **AML-1 (2.60 eV) > AML-2 (2.23 eV) > AML-3 (2.17 eV) > AML-4 (1.92 eV)**. This order supports the fact that strong electron-pulling moieties lead to a lower energy gap between bands. The energy gap of the bands of **AML-4** was the lowest as the presence of an auxiliary electron-withdrawing peripheral electron-pulling moiety with extended conjugation. The inclusion of various acceptors in **AML-1-4**, which is equipped with ethyl carbazole, contributes to its small bandgap energies (Eg). This, in turn, enhances the dye's light-harvesting capability and facilitates easier electron excitation, and also increased photon absorption, resulting in a higher photocurrent and efficiency [31]. These are considered to be critical factors for high-performance dye-sensitized solar cells.

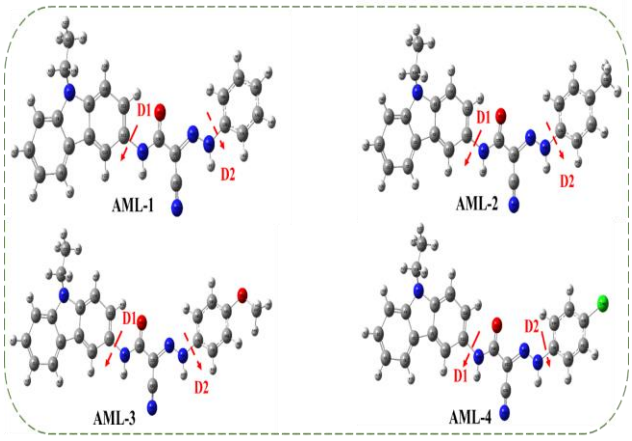

Fig.2. Optimized structure of carbazole sensitizer **AML-1-4**.

Table 3. Molecular parameters of acetohydrazonyl sensitizer **AML-1-4.**

Dyes	*HOMO*	*LUMO*	E_g	*IP*	*EA*	*(η)*	*(s)*	*(χ*	*μ*
AML-1	**-6.27**	**-3.67**	**2.60**	**6.27**	**3.67**	**1.30**	**0.76**	**4.97**	**-4.97**
AML-2	**-5.88**	**-3.65**	**2.23**	**5.88**	**3.65**	**1.11**	**0.90**	**4.76**	**-4.76**
AML-3	**-5.77**	**-3.60**	**2.17**	**5.77**	**3.60**	**1.08**	**0.92**	**4.68**	**-4.68**
AML-4	**-5.49**	**-3.57**	**1.92**	**5.49**	**3.57**	**0.96**	**1.04**	**4.53**	**-4.53**

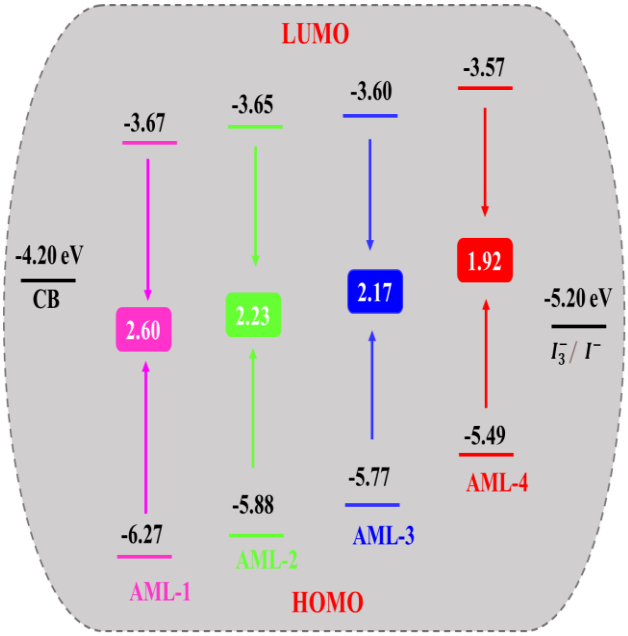

Fig.3. Calculated energy level diagram for carbazole sensitizer **AML-1-4**

3 ***Molecular description parameters for sensitizers (*AML-1-4*).*** Molecular description parameters allow of the synthesized sensitizers by calculating several important parameters inserted in table 3 and calculated from equation (1-5), which in accordance with Koopmans' hypothesis framework [32]. The values of those parameters are particularly critical in determining the reactivity and ability of using of acetohydrazonoyl cyanide sensitizers (**AML-1-4**) in sensitizing solar cell.

$$IP = -E_{HOMO} \quad (1)$$

$$EA = -E_{LUMO} \quad (2)$$

$$\eta = \left(\frac{E_{LUMO} - E_{HOMO}}{2}\right) \quad (3)$$

$$s = \left(\frac{1}{\eta}\right) \quad (4)$$

$$\chi = -\mu = -\left(\frac{E_{LUMO} + E_{HOMO}}{2}\right) \quad (5)$$

The *IP* values of the investigated molecules followed this trend: **AML-4 < AML-3 < AML-2 < AML-1.** The chloro-substituted dye (**AML-4**) had smaller *IP* values than the other substituted dyes (**AML-2-3**) and the unsubstituted dye (**AML-1**). The difference in the values of chemical parameters for the carbazole dyes is related to various electron-withdrawing moieties [33]. The influence of chloro-substituted dye and various π-spacer arrangements on hole and electron transfer and balance was examined. The values of the investigated sensitizers' EA ranged from 3.57 to 3.67 eV. The chemical reactive parameters play a crucial role in designing the molecular structure of light-absorbing materials and are vital for ensuring the stability of the sensitizer and ICT [34]. A better CT, higher efficiency, and higher short-circuit current density (*Jsc*) can be obtained when the η value is lower. Sensitizers **AML-1 (1.30 eV), AML-2 (1.11 eV), AML-3** (1.08 eV), **AML-4** (0.96 eV). **AML-4** exhibited lower η values than the other dyes. In order to enhance the η values, adding (-Cl) to the acceptor and π-spacer components of the dye is recommended, as this has been shown to improve the stability, ICT, and PCE of DSSCs [34]. The electronegativity (χ) of the dyes ranged from 4.53-4.97 eV. Sensitizers with suitable χ and μ values are favorable for DSSCs because they have a greater charge-accepting capacity and electron-donating potential. **AML-1-4** has suitable hardness, electronegativity, and chemical potential for efficient charge transfer and injection, making it a promising sensitizer.

Photovoltaic properties of acetohydrazonoyl cyanide sensitizers AML-1-4.

The research aimed to investigate the influence of substituting groups and employing different π-spacer configurations on the efficiency of (DSSCs). Factors such as light-harvesting capability (LHE), driving force for injection ΔG_{inj}, dye regeneration ΔG_{reg}, recombination driving force ΔG_{rec}, open-circuit voltage (Voc), and short current density (J_{SC}) were scrutinized [35]. Concerning photophysical attributes, the maximum absorption wavelength (λ_{max}) is directly correlated with charge transfer (CT). Sensitizer **AML-4** exhibited a higher λ_{max} compared to **AML-1** and **AML-2** due to its unique π-spacer

arrangement and the presence of a greater number of electron-withdrawing chlorine groups, thereby enhancing electron acceptance and CT. The methoxy substituent in the dye **AML-3** acts as an electron-donating moiety, facilitating increased conjugation and augmenting the electron density on the donor and π-spacer segments, consequently elevating the λ_{max} relative to methyl and unsubstituted analogues. Notably, **AML-4** possessed the lowest energy gap of 1.93 eV, rendering it more suitable for DSSC applications owing to the incorporation of electron-withdrawing groups on the donor and π-spacer components. Furthermore, the light-harvesting efficiency of **AML-4** was marginally higher in comparison to the other sensitizers, as a higher LHE typically translates to an increased (J_{SC}) [36]. The estimated values for the investigated dyes were tabulated in Table 4. As delineated in Table 4, the LHE of the organic dyes ranged from 0.971 to 0.966 eV for the sensitizers **AML-1** to **AML-4**, implying that the incorporation of hetero moieties facilitated an improved photocurrent response. Moreover, critical photovoltaic parameters were computed utilizing equations (**6-11**).

$$\textbf{Where; } E_{OX}^{dye} = -HOMO \quad \textbf{(6)}$$

$$E_{OX}^{dye^*} = E_{OX}^{dye} - E_{0-0} \quad \textbf{(7)}$$

$$\Delta G_{inj}\,(eV) = E_{OX}^{dye^*} - E_{CB} \quad \textbf{(8)}$$

$$\Delta G_{reg}\,(eV) = E_{OX}^{dye} - E_{redox} \quad \textbf{(9)}$$

$$\Delta G_{rec.}\,(eV) = E_{OX}^{dye} - E_{CB} \quad \textbf{(10)}$$

$$V_{OC}\,(eV) = E_{LUMO} - E_{CB} \quad \textbf{(11)}$$

The injection driving force (ΔG_{inj}) and light-harvesting efficiency (LHE) significantly affect the photocurrent (*Jsc*) of the DSSCs. The LHE represents the light absorption capacity. Optimized dyes with high LHE and ΔG_{inj} values enhance electron transport to TiO_2, which is crucial for achieving high *Jsc* and power conversion efficiency [36]. The obtained ΔG_{inj}, for carbazole dye **AML-1-4** were -0.52, -0.56, -0.60 and -0.64 eV, respectively. Notably, all the synthesized sensitizers showed negative ΔG_{inj} values, which are beneficial for electron injection. Sensitizer **AML-4** (0.29 eV) has the highest driving force among the dyes, followed by **AML-3** (**0.57** eV)**, AML-2** (0.**68** eV)**,** and **AML-1** (**1.07** eV) [37]. **AML-4** ted the lowest ΔG_{reg} value of ~ 0.29 eV, demonstrating the maximum dye regeneration capability. The recombination driving force (ΔG_{rec}) values ranged from -1.29 to -2.07 eV. Notably, sensitizer **AML-4** exhibited the lowest ΔG_{rec} of -1.29 eV compared to the other dyes. A lower ΔG_{rec} indicates slower charge recombination kinetics and losses [38]. Based on the analysis of ΔG_{inj}, $\Delta G_{reg,}$ and ΔG_{rec}, carbazole dye **AML-1-4** demonstrated superior properties for DSSCs. (V_{OC}) ranged between (0.53-0.63 eV). The predicted V_{OC} values of the investigated dyes increased in the following order: **AML-1** (**0.53** eV) < **AML-2** (0.**55** eV) < **AML-3** (**0.60** eV) < **AML-4** (**0.63 eV)** for the carbazole sensitizers **AML-1-4** dyes.

***Molecular modeling for acetohydrazonoyl cyanide sensitizers* AML-1-4.** To gain insight for the electronic distribution across the (HOMO) and (LUMO), as well as their respective bandgaps. The HOMO and LUMO energies of molecules serve as indicators of their electron-donating and electron-accepting properties, respectively. **Fig.4** illustrates the importance of (ICT) from the HOMO level (associated with the donor component) to the LUMO level (associated with the acceptor component) [39]. Regarding the sensitizer acetohydrazonyl **AML-1-4**, effective charge separation between the HOMOs and LUMOs was observed. The electron density of the highest occupied molecular orbital (HOMO) is predominantly concentrated on the donor component, specifically the ethyl carbazole segment, whereas the electron density of the LUMO is concentrated on the acceptor moieties, such as phenylhydrazonoyl cyanide, p-tolylhydrazonoyl cyanide, 4-methoxyphenylhydrazonoyl cyanide, and chlorohydrazonoyl cyanide, which include cyano and carbonyl groups. The presence of multiple acceptor and anchoring groups in the **AML-1-4** sensitizers led to greater delocalization of charge in the HOMO and LUMO orbitals. As obvious effective charge transfer between the (HOMO) and (LUMO) which plays a crucial role in the performance of dye-sensitized solar cells. This charge transfer process is responsible for the efficient conversion of light energy into electrical energy within the cell. By optimizing the electron transfer between the HOMO and LUMO, dyes

can enhance their performance in terms of light absorption, charge separation, and overall solar cell efficiency [40].

***Molecular electrostatic potential (MEP) of the acetohydrazonyl sensitizer* AML-1-4.** Molecular electrostatic potential MEP analysis enables the investigation of reactivity in organic molecules and understanding the MEP of dyes consider crucial for comprehending their charge transfer processes, light absorption properties, and overall performance. MEP maps visualize the electrostatic potential on the

molecular surface, with regions of positive potential displayed in blue or green, while negative potential regions are shown in red or orange. These maps help to analyze the electron-donating and electron-accepting capabilities of the dye molecules, as well as identify potential reaction sites and charge distribution patterns [41]. Notably, in the case of acetohydrazonyl **AML-1-4**, the red region in the MEP map was primarily located around the oxygen of the carbonyl group in internal acceptor as shown in Fig.5. Additionally, the red region is present around the cyano and carboxyl groups, as well as the nitrogen of the -CN moiety in all organic dyes. This indicates that these regions are favorable for electrophilic attack. Conversely, the blue zone in the MEP map is situated at the ethyl carbazole moiety, indicating that this region is important for nucleophilic attack.

Table 4. The theoretical photovoltaic parameters of acetohydrazonoyl cyanide AML-1-4.

Dyes	E_{ox}^{dye} (eV)	$E_{ox}^{dye^*}$ (eV)	$E_{0\text{-}0}$ (eV)	ΔG_{inject} (eV)	ΔG_{reg} (eV)	ΔG_{rec} (eV)	(*f*)	LHE (eV)	V_{OC} (eV)
AML-1	6.27	3.68	2.59	-0.52	1.07	-2.07	1.4811	0.966	0.53
AML-2	5.88	3.64	2.24	-0.56	0.68	-1.68	1.4981	0.968	0.55
AML-3	5.77	3.60	2.17	-0.60	0.57	-1.57	1.5350	0.970	0.60
AML-4	5.49	3.56	1.93	-0.64	0.29	-1.29	1.5510	0.971	0.63

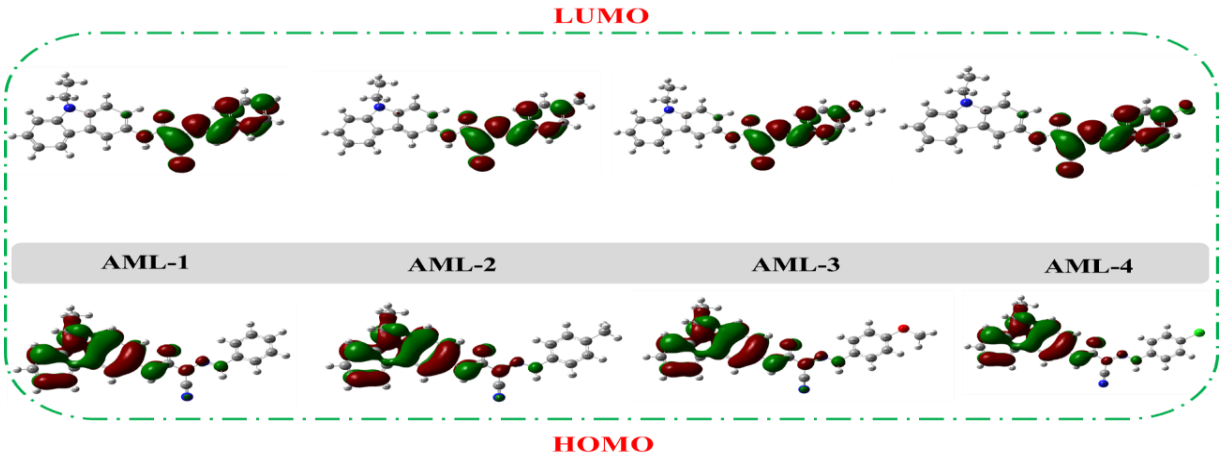

Fig.4. HOMOs and LUMOs geometries for sensitizers **AML-1-4.**

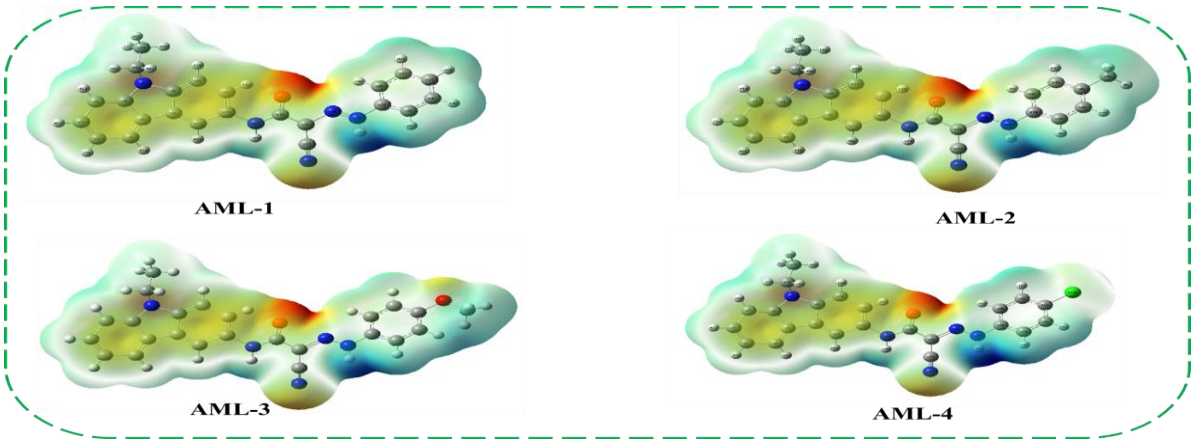

Fig. 5. Molecular electronics (MEP) of carbazole sensitizer **AML-1-4**.

3. Experimental

Synthesis of 2-cyano-N-(9-ethyl-9H-carbazol-3-yl)acetamide (1).

Compound 1 was prepared following the methodology outlined in our previously published research paper **[15].**

General synthesis of the hydrazone derivative **AML-1-4.**

A solution containing p-substituted aniline **2a-d** (0.001 mol) in 0.3 ml concentrated HCl was stirred and cooled to 0–5°C. Diazotization took place by introducing a $NaNO_2$ solution (0.07 g in 5 ml H_2O) into the cooled mixture **[16]**. The resulting fresh diazonium chloride solution was carefully added dropwise to a cold suspension of 2-cyano-N-(9-ethyl-9H-carbazol-3-yl)-acetamide **1** (0.001 mol, 0.27 g) in pyridine (15 ml). Stirring was maintained at 0-5°C for an additional hour and the solid product was collected via filtration. The collected solid was subjected to recrystallization by heating in ethanol, resulting in the formation of **AML-1-4.**

2-((9-Ethyl-9H-carbazol-3-yl)amino)-2-oxo-N-phenylacetohydrazonoyl cyanide (AML-1):

Pale yellow powder, Yield (50 %); m.p. = 208-210°C. IR, cm^{-1}: ν_{max} 3386, 3221 (N-H), 2215 (C≡N) and 1674 (C=O). ^{1}H NMR (ppm): δ 1.31 (t, *J* = 7.50 Hz, 3H), 4.43 (q, *J* = 7.50 Hz, 2H), 7.12 (t, *J* = 7.50 Hz, 1H), 7.18 (t, *J* = 8.00 Hz, 1H), 7.39 (t, *J* = 8.00 Hz, 2H), 7.45 (t, *J* = 8.00 Hz, 1H),7.58-7.60 (dd, *J* = 3.00, 8.50 Hz, 2H), 7.70-7.72 (dd, *J* = 2.00, 9.00 Hz, 1H), 7.76 (d, *J* = 8.00 Hz, 2H), 8.09 (d, *J* = 7.50 Hz, 1H), 8.40 (d, J = 7.50 Hz, 1H), 10.03 (s, 1H), 11.86 (s, 1H).^{13}C NMR (ppm): δ 13.71, 37.01, 108.14, 108.80, 109.22, 111.46, 113.83, 116.18 (2C), 118.67, 120.26, 121.11, 121.80, 122.04, 124.14, 125.83, 129.14 (2C), 129.60, 136.74, 139.99, 142.12, 159.41. Mass analysis (m/z, %): 381 (M^+, 14.73), 369 (17.18), 344 (14.35), 335 (25.30), 321 (14.26), 306 (31.82), 275 (24.95), 271 (17.49), 252 (15.19), 248 (26.62), 240 (18.16), 236 (18.74), 211 (12.32), 203 (12.22), 149 (96.28), 76 (47.86), 69 (68.47), 45 (100.00). Analysis for $C_{23}H_{19}N_5O$ (381.44): Calculated: C, 72.42; H, 5.02; N, 18.36. Found: C, 72.55; H, 5.10; N, 18.44.

2-((9-Ethyl-9H-carbazol-3-yl)amino)-2-oxo-N-(p-tolyl)acetohydrazonoyl cyanide (AML-2):

Orange crystals, Yield (60 %); m.p = 227-229°C. IR (cm^{-1}): ν_{max} 3370, 3218 (N-H), 2207 (C≡N), and 1638 (C=O). ^{1}H NMR (ppm): δ 1.31 (t, *J* = 7.00 Hz, 3H), 2.29 (s, 3H), 4.43 (q, *J* = 7.00 Hz, 2H), 7.17-7.20 (m, 3H), 7.44 (t, *J* = 7.50 Hz, 1H), 7.59 (d, *J* = 8.50 Hz, 2H), 7.65 (d, *J* = 8.00 Hz, 2H), 7.69-7.71 (dd, *J* = 1.50, 8.00 Hz, 1H), 8.09 (d, *J* = 7.00 Hz, 1H), 8.39 (d, *J* = 7.50 Hz, 1H), 9.99 (s, 1H), 11.81 (s, 1H). ^{13}C NMR (ppm): δ 13.73, 20.49, 37.03, 107.43, 108.81, 109.23, 111.61, 113.88, 116.19 (2C), 118.68, 120.27, 121.17, 121.81, 122.06, 125.84, 129.58 (2C), 129.65, 133.36, 136.74, 139.87, 140.00, 159.55. Mass analysis (m/z, %): 395 (M^+, 32.81), 312 (29.82), 267 (6.49), 248 (11.47), 194 (9.48), 180 (11.05), 144 (55.40), 141 (13.54), 134 (49.06), 125 (26.44), 110 (22.73), 105 (12.54), 78 (100.00), 73 (27.94), 68 (27.14), 67 (34.59), 55 (38.95), 51 (44.71). Analysis for $C_{24}H_{21}N_5O$ (395.47): Calculated: C, 72.89; H, 5.35; N, 17.71. Found: C, 72.99; H, 5.30; N, 17.80.

2-((9-Ethyl-9H-carbazol-3-yl)amino)-N-(4-methoxyphenyl)-2-oxoacetohydrazonoyl cyanide (AML-3):

Dark orange powder, Yield (76 %); m.p = 218-220 °C. IR (cm^{-1}): ν_{max} 3373, 3201 (N-H), 2204 (C≡N) and 1638 (C=O). ^{1}H NMR (ppm): δ 1.30 (t, *J* = 7.00 Hz, 3H), 3.75 (s, 3H), 4.43 (q, *J* = 7.00 Hz, 2H), 6.97 (d, *J* = 9.00 Hz, 2H), 7.18 (t, *J* = 7.50 Hz, 1H), 7.44 (t, *J* = 8.50 Hz, 1H), 7.59 (d, *J* = 9.00 Hz, 2H), 7.69-7.71 (m, 3H), 8.08 (d, *J* = 7.00 Hz, 1H), 8.39 (d, *J* = 7.50 Hz, 1H), 9.95 (s, 1H), 11.82 (s, 1H). ^{13}C NMR (ppm): δ 13.72, 37.02, 55.34, 106.60, 108.80, 109.22, 111.80, 113.70, 114.38 (2C), 117.61 (2C), 118.67, 120.25, 121.05, 121.81, 122.05, 125.83, 129.75, 135.77, 136.67, 140.00, 156.35, 159.69. Mass analysis (m/z, %): 411 (M^+, 10.11), 405 (31.03), 397 (45.04), 388 (27.07), 328 (34.72), 319 (42.31), 311 (38.31), 293 (27.78), 269 (29.19), 265 (54.06), 192 (47.64), 157 (48.47), 144 (100.00), 107 (69.34), 97 (46.34), 87 (45.25), 68 (86.98), 57 (54.25).

Analysis for $C_{24}H_{21}N_5O_2$ (411.47): Calculated: C, 70.06; H, 5.14; N, 17.02. Found: C, 70.25; H, 5.10; N, 17.11.

N-(4-Chlorophenyl)-2-((9-ethyl-9H-carbazol-3-yl)amino)-2-oxoacetohydrazonoyl cyanide (AML-4):

Reddish-brown crystals Yield (89 %); m.p = 212-214 °C. IR (cm^{-1}): ν_{max} 3376, 3259 (N-H), 2213 (C≡N) and 1648 (C=O). ^{1}H NMR (ppm): δ 1.31 (t, J = 6.50 Hz, 3H), 4.43 (q, J = 6.50 Hz, 2H), 7.18 (t, J = 7.00 Hz, 1H), 7.44 (d, J = 8.50 Hz, 3H), 7.58-7.60 (dd, J = 2.50, 8.00 Hz, 2H), 7.68-7.70 (m, 1H), 7.79 (d, J = 9.00 Hz, 2H), 8.09 (d, J = 7.00 Hz, 1H), 8.38 (d, J =8.00 Hz, 1H), 10.09 (s, 1H), 11.92 (s, 1H). ^{13}C NMR (ppm): δ 13.72, 37.02, 108.83, 108.92, 109.23, 111.33, 113.93, 117.81 (2C), 118.69, 120.26, 121.18, 121.81, 122.02, 125.85, 127.91, 129.01 (2C), 129.50, 136.87, 139.99, 141.30, 159.22. Mass analysis (m/z, %): 415 (M^+, 6.77), 396 (27.57), 387 (10.41), 332 (29.08), 269 (15.35), 242 (28.89), 196 (14.41), 190 (17.79), 180 (19.10), 167 (30.64), 160 (46.80), 133 (19.44), 71 (100.00), 57 (24.36). Analysis for $C_{23}H_{18}ClN_5O$ (415.88): Calculated: C, 66.43; H, 4.36; N, 16.84. Found: C, 66.58; H, 4.28; N, 16.98.

Conclusion

This study focused on the synthesis and theoretical investigation of four new organic dyes (**AML-1-4**) as photosensitizers for dye-sensitized solar cell applications. Through density (DFT) and DFT (TD-DFT) analyses, various properties and parameters of the dyes were determined, including the energy levels, bandgap, electron affinity, and light-harvesting efficiency. The effects of systematic variations in the donor, π-spacer, and acceptor units on the optical, electronic, and photovoltaic properties were analyzed. Among the synthesized dyes, **AML-4**, which incorporates carbazole as a strong donor and chlorohydrazonoyl cyanide as an acceptor, exhibited the most promising characteristics. It demonstrates a red-shifted absorption spectrum, narrow bandgap, superior electron delocalization, and favorable alignment of frontier orbital energies, facilitating efficient electron transfer processes. Furthermore, comprehensive simulations provide valuable insights into the structure. The superior photosensitizing performance of **AML-4** could be attributed to these factors. Indeed, the utilization of the **AML-4** dye in (DSSCs) holds great promise for enhancing optoelectronic properties and overall energy conversion efficiency compared to other dyes. The unique characteristics and properties of **AML-4** make it a compelling candidate for improving the performance of DSSCs, thereby paving the way for more efficient and sustainable energy conversion technologies.

Acknowledgment

The authors are thankful to Mansoura University, Egypt, for their support under project ID: MU-SCI-23-37

Conflict of interest

No conflict of interest was declared by the authors.

4. References

1 Lee, M. W., Kim, J. Y., Lee, H. G., Cha, H. G., Lee, D. H., & Ko, M. J. (2021), *J. Energy Chem.*, , Vol. **54**, P. 208.

2 Badawy, S. A., Salem, K. E., Fadda, A. A., Abdel-Latif, E., & Elmorsy, M. R., Dyes Pigm., (2024), Vol. **225**, P. 112096.

3 Gong, J., Liang, J., & Sumathy, K., (2012) Renew. Sustain. Energy Rev., , Vol. **16**, p. 5848.

4 Wu, W., Wang, J., Zheng, Z., Hu, Y., Jin, J., Zhang, Q., & Hua, J., (2015) Sci. Rep., , Vol. **5**, P. 8592.

5 Panwar, N. L., Kaushik, S. C., & Kothari, S., (2011) Renew. Sustain. Energy Rev., , Vol. **15**, P.1513.

6 Britel, O., Fitri, A., Benjelloun, A. T., Slimi, A., Benzakour, M., & Mcharfi, M., (2022) *J. Photochem. Photobiol*, , Vol. **429**, p. 113902.

7 Hosseinnezhad, M., Nasiri, S., Fathi, M., Ghahari, M., & Gharanjig, K., (2022) Opt. Mater., , Vol. **124**, P. 111999.

8 Radwan, A. S., Elmorsy, M. R., Abdel-Latif, E., Makhlouf, M. M., & Badawy, S. A., (2023) Opt. Mater., , Vol. **140**, P. 113914.

9 Rashid, M. A. M., Hayati, D., Kwak, K., & Hong, J. (2020), *J. Nanomater.*, , Vol. **10**, P. 914.

10 Juma, J. M., Vuai, S. A. H., & Babu, N. S. (2019) , *Int. J. Photoenergy*,.

11 Han, L., Zu, X., Cui, Y., Wu, H., Ye, Q., & Gao, J. (2014) , Org. Electron., , Vol. **15**, P. 1536.

12 Elmorsy, M. R., Abdelhamed, F. H., Badawy, S. A., Abdel-Latif, E., Abdel-

Shafi, A. A., & Ismail, M. A., (2023) Sci. Rep., , Vol. **13**, P. 13825.
13 Dwivedi, S., Bardhan, S., Ghosh, P., & Das, S., (2014), *RSC Adv*., Vol. **4**, P. 41045.
14 Elmorsy, M. R., Badawy, S. A.,Alzahrani, A. Y., & El-Rayyes, A., (2023*)* Opt. Mater., , Vol. **135**, P. 113359.
15 Mostafa, A. R., Badawy, S. A., Abdel-Latif, E., Fekri, A., Fadda, A. A., & Elmorsy, M. R., (2024) *J. Photochem. Photobiol., A*, , Vol. **450**, P. 115478.
16 Gomha, S. M., Abdelrazek, F. M., Abdelrahman, A. H., & Metz, P. (2018), *J. Heterocycl. Chem.*, , Vol. **55**, P. 1729.
17 Wu, G., Kong, F., Zhang, Y., Zhang, X., Li, J., Chen, W.,. & Dai, S. (2014), Dyes Pigm., Vol. **105**, p. 1.
18 Elmorsy, M. R., Lyu, L., Su, R., Abdel-Latif, E., Badawy, S. A., El-Shafei, A., & Fadda, A. A. (2020) , Photochem. Photobiol. Sci., , Vol. **19**, P. 281.
19 El-Shafeai, H. M., Badawy, S. A., Ismail, M. A., Abdel-Latif, E., Fadda, A. A., & Elmorsy, M. R. (2023), RSC Adv., , Vol. **13**, P. 9720.
20 Elmorsy, M. R., Badawy, S. A., Salem, K. E., Fadda, A. A., & Abdel-Latif, E. (2023), *J. Photochem. Photobiol., A*, , Vol. **436**, P. 114421.
21 Frisch, M J., Trucks, G. W., Schlegel, H. B., Scuseria, G. E., Robb, M. A., Cheeseman, J. R., Scalmani, G., Barone, V., Mennucci, B., Petersson, G. A., Nakatsuji, H., Caricato, M., Li, X., Hratchian, H. P., Izmaylov, A. F., Bloino, J., Zheng, G., Sonnenberg, J. L., Hada, M., Ehara, M., Toyota, K., Fukuda, R., Hasegawa, J., Ishida, M., Nakajima, T., Honda, Y., Kitao, O., Nakai, H., Vreven, T., Montgomery Jr., J. A., Peralta, J. E., Ogliaro, F., Bearpark, M., Heyd, J. J., Brothers, E., Kudin, K. N., Staroverov, V. N., Kobayashi, R., Normand, J., Raghavachari, K., Rendell, A., Burant, J. C., Iyengar, S. S., Tomasi, J., Cossi, M., Rega, N., Millam, J. M., Klene, M., Knox, J. E., Cross, J. B., Bakken, V., Adamo, C., Jaramillo, J., Gomperts, R., Stratmann, R. E., Yazyev, O., Austin, A. J., Cammi, R., Pomelli, C., Ochterski, J. W., Martin, R. L., Morokuma, K., Zakrzewski, V. G., Voth, G. A., Salvador, P., Dannenberg, J. J., Dapprich, S., Daniels, A. D., Farkas, O., Foresman, J. B., Ortiz, J. V., Cioslowski, J. and Fox, D. J., (2009) Gaussian 09, Revision A.02, Gaussian, Inc., Wallingford CT,.
22 Elroby, S. A., & Jedidi, A. (2020), Struct. Chem., Vol. **31**, P. 1125.
23 Saputra, R. M., Yang, C., Zhao, D., Zheng, X., & Li, Y., (2022) Comput. Theor. Chem., , Vol. **1207**, P. 113467.
24 Khalid, M., Ali, A., Khan, M. U., Tahir, M. N., Ahmad, A., Ashfaq, M., & Braga, A. A. C. (2021), *J. Mol. Struct.*, Vol. **1230**, P. 129827.
25 Mubashar, U., Farhat, A., Khera, R. A., Iqbal, N., Saleem, R., & Iqbal, J. (2021), *J. Mol. Model.*, , Vol. **27**, P. 216.
26 Pasha, A. R., Khalid, M., Shafiq, Z., Khan, M. U., Naseer, M. M., Tahir, M. N., & Jawaria, R., (2021) *J. Mol. Struct.*, Vol. **1230**, P. 129852.
27 Krishnan, K. G., Sivakumar, R., Thanikachalam, V., & Saleem, H., (2015) Spectrochim. Acta, Part A, , Vol. **144**, P. 29.
28 Wang, J., Li, H., Ma, N. N., Yan, L. K., & Su, Z. M. (2013). Dyes Pigm., 2013, ***99*(2),** 440-446.
29 Amiri, S. S., Makarem, S., Ahmar, H., & Ashenagar, S. (2016) , *J. Mol. Struct.*, , Vol. **1119**, P. 18.
30 Elmorsy, M. R., Su, R., Abdel-Latif, E., Badawy, S. A., El-Shafei, A., & Fadda, A. A. (2020), *J. Mater. Sci.: Mater. Electron.*, , Vol. **31,** P. 7981.
31 Elmorsy, M. R., Abdelhamed, F. H., sultan Alqahtani, A., Abdel-Latif, E., Abdel-Shafi, A. A., & Ismail, M. A., (2024) Opt. Mater., , Vol. **151**, P. 115386.
32 Elmorsy, M. R., Abdel-Latif, E., Gaffer, H. E., Badawy, S. A., & Fadda, A. A. (2022), *J. Mol. Struct.*, , Vol. **1255**, P. 132404.
33 Zahid, S., Rasool, A., Ans, M., Yaseen, M., & Iqbal, J. (2021), Energy & Fuels, , Vol. **35**, P. 15018.
34 Ouared, I., Rekis, M., & Trari, M., (2021) Dyes Pigm., , Vol. **190**, P. 109330.
35 Khalid, M., Ali, A., Jawaria, R., Asghar, M. A., Asim, S., Khan, M. U., ... &

Akram, M. S., (2020) RSC Adv., , Vol. **10**, P. 22273.
36 Zhang, J., Lu, F., Qi, S., Zhao, Y., Wang, K., Zhang, B., & Feng, Y., (2016) Dyes Pigm., , Vol. **128**, P. 296.
37 Badawy, S. A., Su, R., Fadda, A. A., Abdel-Latif, E., El-Shafei, A., & Elmorsy, M. R. (2022). Optik, 249, 168274.
38 Badawy, S. A., Abdel-Latif, E., Assiri, M. A., Ali, T. E., & Elmorsy, M. R. (2023), Dyes Pigm., Vol. **217**, P. 111447.
39 Janjua, M. R. S. A., Khan, M. U., Khalid, M., Ullah, N., Kalgaonkar, R., Alnoaimi, K., ... & Jamil, S. (2021),, *J. Cluster Sci.*, Vol. **32**, P. 243.
40 Naik, P., Su, R., Elmorsy, M. R., Babu, D. D., El-Shafei, A., & Adhikari, A. V. (2017), *J. Photochem. Photobiol.*, A, , **345**, 63-73.
41 Badawy, S. A., Abdel-Latif, E., Fadda, A. A., & Elmorsy, M. R. (2022), Sci. Rep., , Vol. **12**, P. 12885.